CHAPTER III
SYNTHESIS OF MCM-48 FROM SILATRANE VIA SOL-GEL PROCESS

3.1 Abstract

High-quality cubic MCM-48 is successfully synthesized using a new silica source known as silatrane and cetyltrimethylammonium bromide (CTAB) as the structure-directing agent via sol–gel process. The effects of synthesis parameters, viz. crystallization temperature, crystallization time, surfactant concentration, quantity of NaOH, and silica source, on the product structure are investigated. The synthesized samples are characterized using X-ray diffractometer (XRD), N_2 adsorption–desorption isotherms, and electron microscopy. Optimally, this product is synthesized from samples crystallized at 140°C for 16 h with a CTAB/SiO_2 ratio of 0.3 and NaOH/SiO_2 ratio of 0.5. The XRD result exhibits a well-resolved pattern, corresponding to the *Ia3d* space group of MCM-48. The BET surface area of this product is as high as 1,300 m^2/g with a narrow pore-size distribution of 2.86 nm. The scanning electron microscopic (SEM) images also show the truncated octahedral shape and well-ordered pore system of MCM-48 particles.

(**Keywords**: MCM-48; Silatrane; Sol–gel process; Truncated octahedral shape)

3.2 Introduction

Since 1992 after mesoporous molecular sieves in M41S family were discovered by Mobil's group [1, 2], these materials have attracted remarkable attentions due to its high surface area, ordered pore structure array, and narrow pore size distribution [3]. There are three categories of M41S divided by the different arrays, viz. hexagonal (MCM-41), cubic (MCM-48), and lamellar (MCM-50) [4, 5]. Among them, MCM-48 is a more attractive candidate as a catalyst, catalyst support, adsorbent, or template for synthesis of advanced nanostructures, probably owing to its unique three-dimensional pore structure. The cubic MCM-48 indexed in the space group of *Ia3d* is the most interesting in terms of catalytic activity because it has a three-dimensional pore structure which reduces the diffusion limitations and avoids the pore-blocking of the catalysts [6].

Although MCM-48 is a more attractive candidate as a catalyst support or adsorbent than MCM-41, its success is curtailed by the lengthy reaction times and rigorous conditions required for its synthesis. The cubic MCM-48 is an intermediate during the transformation from hexagonal to lamellar phases; thus, the synthesis conditions must be carefully controlled. Silica sources are also found to affect the MCM-48 formation, as studied by Xu *et al.* [7], resulting in different silica structures. Therefore, most researchers have mainly focused on MCM-41 rather than MCM-48 [8–13]. Furthermore, a high surfactant amount and additives are required to obtain the cubic *Ia3d* MCM-48 mesoporous structure. To date, many researchers have tried to minimize the surfactant amount in many ways, using such means as organic additives [14, 15] or salts (i.e. NaF and Na_2SO_4) [16, 17]. Generally, to obtain MCM-48, the most widely used raw materials are CTAB as a surfactant, NaOH as a catalyst, and tetraethylorthosilicate (TEOS) as a silica source, using conventional autoclave heating for several days. According to the materials safety data sheets (MSDS), however, TEOS presents significant handling problems due to such factors as high toxicity and moisture sensitivity. In this research, we introduce another source of silica known as silatrane. Silatrane can be easily synthesized from inexpensive and commercially available starting materials, namely, silicon dioxide

and triethanolamine, in ethylene glycol solvent [18, 19]. One unique characteristic of silatrane is a moisture stability lasting up to several weeks, thus allowing for control of the hydrolysis rate during sol–gel processing.

In previous works, we successfully synthesized many microporous [20–23] and mesoporous [24–28] zeolites via sol–gel process, using moisture stable metal alkoxides for example silatrane, alumatrane, cerium glycolate, zirconium glycolate as the precursors. In this work, we systematically studied the effects of crystallization temperature, crystallization time, surfactant concentration, amount of NaOH, and silica source on the product structure to obtain the optimum synthesis conditions of MCM-48.

3.3 Experimental

3.3.1 Synthesis of Silatrane

Following Wongkasemjit's synthetic method [29], silatrane was synthesized by mixing 0.1 mol fumed silica (99.8%, Sigma–Aldrich, St. Louis, MO), 0.125 mol triethanolamine (TEA; QREC, New Zealand), and 100 ml ethylene glycol (EG; J.T. Baker, Philipsburg, NJ). The reaction was refluxed at 200°C under nitrogen atmosphere for 10 h in oil bath. The excess of EG was removed under vacuum at 110°C to obtain a crude brown solid. The obtained product was purified by using acetronitrile (Labscan, Bangkok, Thailand) to remove any TEA and EG residues. The white silatrane product was vacuum-dried overnight before characterization by Fourier transform infrared absorption spectrometry (FT-IR, Bruker Optics EQUINOX55) at a resolution of 2 cm^{-1}, and by thermogravimatric analysis (TGA, Perkin-Elmer instruments) using a heating rate of 10°C/min from room temperature to 650°C in a nitrogen atmosphere. The FT-IR bands observed were 3,000–3,700 cm^{-1} (w, νO–H), 2,860–2,986 cm^{-1} (s, νC–H), 1,244–1,275 cm^{-1} (m, νC–N), 1,170–1,117 cm^{-1} (bs, νSi–O), 1,093 cm^{-1} (s, νSi–O–C), 1,073 cm^{-1} (s, νC–O), 1,049 cm-1 (s, νSi–O), 1,021 cm^{-1} (s, νC–O), 785 and 729 cm^{-1} (s, νSi–O–C), and 579 cm^{-1} (w, νN→Si). TGA exhibited one sharp mass loss at 390°C and gave a 19% ceramic yield, corresponding to $N(CH_2CH_2O)_3Si–OCH_2CH_2–N(CH_2CH_2OH)_2$.

3.3.2 Synthesis of MCM-48

To synthesize this material, CTAB (Sigma–Aldrich) was dissolved in a solution containing water and 2 M NaOH. The mixtures were vigorously stirred with slight heating to dissolve surfactant. Then, silatrane precursor was added, followed by stirring for 1 h. The molar composition of the gel was 1.0 SiO_2:xCTAB:0.50NaOH:62.0H_2O, where $0.15 \leq x \leq 0.65$. The resulting mixture was transferred to a Teflon-lined stainless steel autoclave and treated at 130–150°C for a certain time in a range of 12–24 h. The resulting solid product was collected by filtration and dried overnight at ambient conditions. The removal of the surfactant was performed by calcination at 550°C for 6 h (Carbolite, CFS 1200, Hope Valley, UK) at a heating rate of 0.5°C/min to obtain mesoporous MCM-48. In this study, crystallization time and temperature, surfactant concentration, alkalinity, and silica source were varied.

3.3.3 Characterization

The mesoporous products were characterized using a Rigaku X-ray diffractometer (XRD, Tokyo, Japan) and CuKα radiation in the range of 2h = 2–8° at a scanning speed of 1°C/min, 40 kV, and 30 mA. MCM-48 morphology was carried out by a field emission scanning electron microscope (FE-SEM, Hitachi/S-4800) and the samples shadowed with platinum. The order of mesopores was investigated using a transmission electron microscope (TEM, JEOL 2010F). The surface area and average pore size were estimated by the Brunauer-Emmett-Teller (BET) method on a Quantasorb JR instrument (Mount Holly, NJ).

3.4 Results and Discussion

3.4.1 Effects of Crystallization Time and Temperature

The crystallization time and temperature are the important key factors in synthesizing MCM-48, due to a consecutive transformation of MCM-48 via hexagonal to cubic and lamellar phases. Thus, these studies were attempted at 130,

140, and 150°C for various times using a gel molar composition of SiO_2:0.65CTAB:0.5NaOH:62H_2O and silatrane as silica source.

The results of the as-synthesized samples obtained at 17, 19, and 24 h showed that MCM-48 started to form at 130°C for 24 h (not shown). However, upon calcination, poor-resolved diffraction peaks were obtained probably due to either a too-low crystallization temperature or a too short crystallization time to form MCM-48 since all three samples showed the dominance of the hexagonal phase (MCM-41). When the crystallization temperature increased to 140°C, the samples that were heated for 16 h and above showed the diffraction (220) characteristic peak of MCM-48 (Fig. 3.1). However, the occurrence of mixed phase of the cubic and the lamellar phases was observed from the sample heated for 24 h, as shown in Fig. 3.1a. The results are in good agreement with those described by Kruk *et al.* [30],who also showed a significant difference of XRD patterns between a pure cubic MCM-48 and a mixed phase when they synthesized MCM-48 at 150°C for 1 day. They found that the (220) peak of MCM-48 overlapped with the (001) peak of the lamellar phase, resulting in a broad peak of (220), along with (211), (420), and (332) peaks of MCM-48, and a broad (002) peak of the lamellar phase. In addition, as crystallization time increased, the first dominant peak of (211) started to lose its intensity while the peaks of (001) and (002) increased, indicating that the lamellar phase of MCM-50 had begun to develop, as found by Roth [31]. In contrast to the sample crystallized for 12 h at 140°C, it showed a mixed phase between the hexagonal and the cubic phases, hinting at a relationship to the cubic phase (see Fig. 3.1a, 12 h). Furthermore, the structure was not strongly established, and it deteriorated considerably upon calcination, as shown by a poor-quality XRD pattern (Fig. 3.1b, 12 h). The results demonstrated that the samples synthesized at 140°C for 16 and 20 h were crystallized completely. The XRD patterns of the calcined samples synthesized for 16–24 h exhibited a significant increase in the intensity of peaks, indicating that an atomic reorganization occurred during the removal of the surfactant molecules in the calcination process, and the degree of ordering was enhanced [32, 33]. Another attempt was performed at 150°C of the crystallization temperature for the desired

length of time (17–24 h) and failed to obtain pure MCM-48. Instead, a mixed phase between the lamellar and the cubic phases was obtained (not shown).

The XRD patterns of the calcined samples, compared to the as-synthesized samples, were shifted to the higher value of 2-theta, meaning that the contraction of the lattice occurred during the process of removing surfactant because of the condensation of silanol groups on the wall [34].

The samples synthesized for different periods of time were characterized further by N_2-adsorption and desorption isotherms, as illustrated in Fig. 3.2. According to IUPAC classification, all samples showed a typical type IV isotherm, consisting of three stages. At low relative pressure of $P/P_0<0.2$, the lines can be extrapolated to the origin due to monolayer adsorption of nitrogen on the walls of the mesopores. This confirms the absence of any detectable micropore filling at low partial pressure [33]. In the region of P/P_0 = 0.2–0.3, a steep in isotherms was observed, as a result of the capillary condensation in the mesopores, indicating a uniform pore-size distribution and a highly ordered pore structure. This can also be confirmed by calculating pore-size distribution with BJH method by using the desorption branch of isotherms, as given in Fig. 3.2 inset. The peak showing a very narrow pore-size distribution with a peak maximum of about 2.3 nm was observed. After the relative pressure P/P_0~0.3, the isotherm was almost flat owing to multilayer adsorption on the outer surface of the particles, as can be seen in Fig. 3.2a [35, 36]. Additionally, the absence of hysteresis loop in Fig. 3.2a was observed, which can be attributed to the small size of the particles [33]. On the contrary, in Fig. 3.2b, c, the presence of a triangular hysteresis loop at relative pressure of 0.5–1 on the isotherms indicates the contamination with the lamellar phase after calcinations, leading to the lower surface area [30], as shown in Table 3.1. In agreement with the study of Kruk *et al.* [30], they showed a decrease of surface area from 1,240 m^2/g for a pure MCM-48–840 m^2/g for a mixed lamellar phase. These results also agree with Sing *et al.* [37], who suggested that this type of hysteresis loop represented a slit-shaped pore or plate-like particle. In addition to the surface area, the pore volume also decreased with increased time, contributing to a collapsed lamellar phase upon calcinations [38]. From these studies, it can be

concluded that the crystallization temperature of 140°C for 16 h is suitable for synthesizing MCM-48, and an increase in crystallization temperature accelerated the rate for crystallite formation while shortening the time.

3.4.2 Effect of Surfactant Concentration

The effect of CTAB concentration was investigated by preparing samples with different molar gel compositions of SiO2:xCTAB:0.5NaOH:62H_2O, where $0.15 \leq x \leq 0.65$. The study was carried out at 140°C for 16 h. Due to the environmental concerns, the surfactant amount should be minimized. In addition, when compared to higher ratios, the low surfactant/silicon ratio provides several advantages, such as increased wall thickness, improved stability of the entire mesostructure, and prevention of structural collapse during calcinations [15].

When the ratio of CTAB/SiO_2 was kept at 0.65, the cubic MCM-48 was obtained. Similar results were reported for the system using the formula TEOS-0.5NaOH- 0.65CTACl-62H_2O at 100°C for 3 days [6]. The XRD patterns in Fig. 3.3 show that the cubic MCM-48 can be obtained in the CTAB/SiO_2 ratio range of 0.2–0.65, whereas the hexagonal MCM-41-type mesoporous silica material was formed at the CTAB/SiO_2 ratio equal to 0.15.The formation of MCM-48 even at a low CTAB-to-SiO_2 ratio can be explained using the surfactant packing parameter [15, 36], g, determined by the following equation;

$$g = V/ (a_0L)$$

where V is the total volume of surfactant chains plus any co-solvent (organic molecules), a_0 is the effective headgroup area at the organic–inorganic interface, and L is the length of motional surfactant tail. Small values of g stabilize more curved surfaces, such as MCM-41, which has a g value between 1/3 and 1/2, while g = 1 stabilizes layers and larger values stabilize structures with less curvature, such as MCM-48, having a g value between 1/2 and 2/3.

When considering the sol–gel processing of the silatrane precursor, TEA molecules are generated in the mixture as a by-product via the hydrolysis reaction. The TEA molecules stay in the hydrophilic region of the surfactant molecules [39] due to the hydroxyl groups of the molecule, causing more effective polar head-group area of the CTA^+ micelle, resulting in a decrease of a_0. From the equation for calculating the parameter g, g is inversely proportional to a_0, thus, a decrease of a_0 increases g, which is favorable for the cubic MCM-48 formation. This suggests that MCM-48 can be successfully synthesized with use of the silatrane precursor even if the concentration of CTAB is low, and there is no need to include other additives in the system.

From Fig. 3.3, the XRD pattern of using 0.3 mol CTAB exhibits a well-resolved secondary diffraction at above 3.5 degrees of 2-theta, indicating a highly long range order of this material, as compared to other ratios. Lysenko and coworkers [40] also synthesized MCM-48 with a CTAB/TEOS ratio of 0.3; but the reaction was performed at 100°C for 3 days. In our work, at the same ratio, a much shorter reaction time is required at a higher temperature. The N_2-adsorption and desorption result also shows nice isotherms and pore-size distribution (see Fig. 3.4).

In our study, the pore volume and *d* spacing decreased as the surfactant/silicon ratio ($x>0.35$) increased, whereas the surface area increased (Table 3.2). The trend was similar to the results obtained from Yu *et al.* [41] who varied a surfactant/silicon ratio from 0.1 to 0.25 at 110°C for 72 h. When surfactant/silicon ratio increased, there was no slit-shaped pores or plate-like particles of the solid, as observed from the disappearance of a hysteresis loop between $P/P_0 = 0.4$ and 1 in the adsorption–desorption isotherms (Fig. 3.2a) whereas the lower surfactant/silicon ratio provided a hysteresis loop, implying that the complementary inter-particles appeared in a mesoporous structure, leading to an increase of pore volume. Moreover, the decrease of the *d* spacing with an increase in surfactant/silicon ratio was resulted from a thinner wall and a decreasing of pore size obtained when increasing the surfactant concentration to form liquid crystals [41]. Additionally, the *d* spacing increased in the surfactant/silica ratio range of 0.25-0.35. These can be described in term of micelle formation. As the surfactant concentration increased

from 0.25 to 0.35, the surfactants was more participated in the individual micelle leading to increasing the size of micelles as well as the *d* spacing. However, as the surfactant concentration increased to a certain point (x>0.35), the excessive amount of surfactants led to the increasing number of micelles instead of increasing micelle size, resulting in the decreasing of *d* spacing [42]. However, conversely, the increase of the surface area with an increase in surfactant/silicon ratio can be described in terms of the smaller size of particles. According to the Scherrer equation, particle sizes of MCM-48 synthesized by using 0.3 and 0.65 mol of CTAB were found to be 110.8 and 92.3 nm, respectively. In addition, as the surfactant concentration increased, the redundant surfactant could be adsorbed on the surface of particles of MCM-48 which reduced the surface tension and prevented the aggregation of particles evidenced indirectly by the disappearance of hysteresis loop. Therefore, the external surface area increased, resulting in the increase of the total surface area. In the range of $0.3 \leq x \leq 0.65$, the surface areas of our samples were slightly different. When x was less than 0.3, the surface area and the intensity of XRD patterns (Fig. 3.3) decreased, resulting from too low surfactant concentration to form a well-ordered of MCM-48. Instead, MCM-41 was obtained at 0.15 surfactant/silica ratio, meaning that this concentration is not enough to form MCM-48.

3.4.3 Effect of The Alkalinity

Another important parameter examined was the alkalinity in the synthesis gel ascertained by NaOH concentration. To study this effect, the synthetic gel was prepared, using the formula of SiO_2:0.3 CTAB:y NaOH:62 H_2O, where $0.45 \leq y \leq 0.55$. The OH^-/Si ratio was varied as 0.45, 0.5, and 0.55. Figure 3.5a shows XRD patterns of MCM-48 with various amounts of NaOH. All these samples revealed a well-resolved pattern of the *Ia3d* cubic MCM-48. However, as shown in Fig. 3.5b, although all samples illustrate the capillary condensation step at P/P_0 of 0.2–0.3 belonging to MCM-48, the samples prepared from using the NaOH concentration above 0.45 seem to have the lamellar phase mixing with MCM-48, as indicated by the presence of the hysteresis loop, which is consistent with the study of

Kruk *et al.* [30]. This suggests that a high concentration of alkali probably drives the reaction to go further to the lamellar phase, as also suggested by Behrens *et al.* [43]. Moreover, the pore size and the pore volume decreased with an increase in the OH^- /Si ratio (see Table 3.3), consistent with the results obtained by Collart *et al.* [44] who synthesized MCM-48 using a molar gel composition of Si:xOH^-: 100H_2O:0.1GEM 16-12-16, where x = 0.2 and 0.26 at 130°C for 3 days, and found that a reduction of the OH^-/Si ratio increased the pore diameter of the calcined MCM-48 samples. As a conclusion and in agreement with Behrens *et al.* [43], the formation of the lamellar phase of MCM-50 was encouraged by using higher synthesis temperatures, higher basicities of the synthesis solutions, and longer reaction times.

3.4.4 Effect of Silica Source

We also performed the same reaction conditions with a traditional silica source such as TEOS instead of the silatrane precursor, and found that the crystalline phase of MCM-48 could not be obtained. This result can be explained in terms of the property of the material itself. TEOS is very sensitive to the reaction so it can be hydrolyzed very quickly, as compared to the moisture-stable silatrane. Consequently, the addition of ethanol is usually required for the synthesis of MCM-48 in the TEOS system to retard the hydrolysis reaction and also to increase a surfactant packing parameter, as described elsewhere [45, 47]. Moreover, the longer crystallization time is needed for the phase transformation from hexagonal to cubic phases; thus, the MCM-48 could not be obtained within 16 h. In contrast to the synthesis of MCM-48 using the silatrane precursor, the TEA molecules, the by-product after the hydrolysis process, can improve a surfactant packing parameter, as discussed earlier. Moreover, there is no need to add ethanol into the system since the hydrolysis rate of the silatrane is not as fast as the TEOS. It could be inferred that the silatrane is a good candidate as a silica source for the synthesis of high quality MCM-48 with a lower surfactant/silica ratio for a shorter crystallization time.

3.4.5 Electron Microscopic Results of MCM-48 Samples

3.4.5.1 Field Emission Scanning Electron Microscopy

The samples synthesized in this work were examined by FE-SEM to investigate their morphology. The images in Fig. 3.6 are the sample synthesized with a molar gel composition of SiO_2:0.3CTAB:0.5NaOH:62H_2O at 140 °C for 16 h, and exhibit the truncated octahedral shape of aggregated MCM-48 particles, consistent with the results observed by Diaz *et al.* [45] and Alfredsson *et al.*[46]. Diaz *et al.* obtained this shape when they synthesized with SiO_2:0.65CTAB:0.5NaOH:120H_2O:4.7EtOH at 140°C for 20 h, and after prolonging the reaction time to 48 h, the lettuce-like morphology, corresponding to lamellar phase of MCM-50, was obtained; whereas, Alfredsson *et al.* synthesized the truncated octahedral shape of MCM-48 using TEOS:0.65CTACl:0.5NaOH:62H_2O at 95°C for 3 days.

In our case, as CTAB concentration increased from 0.3 (Fig. 3.6) to 0.65 (Fig. 3.7) mol, FE-SEM images of the synthesized MCM-48 did not show only the truncated octahedral shape, as did those prepared from 0.3 mol CTAB. The image obtained from the mixture heated for 24 h crystallization time (Fig. 3.7a) shows an especially mixed morphology of the truncated octahedral shape and the lettuce-like morphology. It can be inferred that the molar ratio of CTAB to SiO_2 indeed affects the MCM-48 formation. These results are consistent with the N_2-adsorption and desorption isotherms of the calcined samples prepared at 140°C for various times (see Fig. 3.2b, c). On the contrary, the lettuce-like morphology disappeared in the sample prepared with the CTAB/SiO_2 ratio equal to 0.3, suggesting that a lamellar phase (MCM-50) required a higher surfactant-to-silica ratio and a longer synthesis time.

3.4.5.2 Transmission Electron Microscopy

Figure 3.8 shows the TEM images of the MCM-48 sample synthesized with a molar gel composition of SiO_2:0.3CTAB:0.5NaOH:62H_2O at

140°C for 16 h. Figure 3.8a shows the pore structure along the cubic [100] direction with a uniform channel system, consistent with the reports from Xu *et al.* [33] and Schumacher *et al.* [47]. Nonetheless, the [111] direction, see Fig. 3.8b, exhibits a well-defined hexagonal arrangement [33] and continuous channels running through the structure [48].

3.5 Conclusions

A novel silica source known as silatrane has been successfully used for synthesis of MCM-48 with high surface area and narrow pore-size distribution. XRD, SEM, and TEM indicate a well-ordered structure of MCM-48 with a truncated octahedral shape. The results also show that all synthesis parameters studied have a considerable effect on the synthesis of MCM-48. The optimum synthesis condition for synthesizing MCM-48 is as follows; SiO_2:0.3CTAB: 0.5NaOH:62H_2O at 140°C for 16 h. The lower amount of CTAB is needed due to the TEA molecules generated from the silatrane precursor, causing higher surfactant packing parameter of micelle which is preferable for the cubic phase.

3.6 Acknowledgements

This research is financially supported by the Thailand Research Fund and the Center for Petroleum, Petrochemicals, and Advanced Materials, Chulalongkorn University, Thailand. The authors would like to thank Mr. John M. Jackson for English proofreading.

3.7 References

[1] Kresge, C.T., Leonowicz, M.E., Roth, W.J., Vartuli, J.C., and Beck J.S. (1992) Ordered mesoporous molecular sieves synthesized by a liquid-crystal template mechanism. Nature, 359, 710-712.

[2] Beck, J.S., Vartuli, J.C., Roth, W.J., Leonowicz, M.E., Kresge, C.T., Schmitt, K.D., Chu, C.T.W., Olson, D.H., Sheppard, E.W., McCullen, S.B., Higgins, J.B., and Schlenker, J.L. (1992) A new family of mesoporous molecular sieves prepared with liquid crystal templates. J. Am. Chem. Soc. 114, 10834-10843.

[3] Shao, Y., Wang, L., Zhang, J., and Anpo, M. (2005) Novel synthesis of high hydrothermal stability and long-range order MCM-48 with a convenient method. Micropor. Mesopor. Mater., 86, 314.

[4] Sayari A. (1996) Catalysis by Crystalline Mesoporous Molecular Sieves. Chem Mater, 8, 1840–1852.

[5] Vinu A., Murugesan V., Hartmann M. (2003) Pore Size Engineering and Mechanical Stability of the Cubic Mesoporous Molecular Sieve SBA-1, Chem. Mater., 15, 1385–1393.

[6] Monnier, A., Schüth, F., Huo, Q., Kumar, D., Margolese, D., Maxwell, R.S., Stucky, M., Krishnamurty, G.D., Petroff, P., Firouzi, A., and Janicke, M. (1993) Cooperative Formation of Inorganic-Organic Interfaces in the Synthesis of Silicate Mesostructures.Science, 261, 1299-1303.

[7] Xu, J., Luan, Z., He, H., Zhou, W., and Kevan, L. (1998) A Reliable Synthesis of Cubic Mesoporous MCM-48 Molecular Sieve. Chem. Mater., 10, 3690-3698.

[8] Huo, Q., Margolese, D.I., and Stucky, G.D. (1996) Surfactant Control of Phases in the Synthesis of Mesoporous Silica-Based Materials. Chem. Mater., 8, 1147-1160.

[9] Gallis, K.W. and Landry, C.C. (1997) Synthesis of MCM-48 by a Phase Transformation Process. Chem. Mater., 9, 2035-2038.

[10] Corma, A., Kan, Q., and Rey, F. (1998) Synthesis of Si and Ti-Si-MCM-48 mesoporous materials with controlled pore sizes in the absence of polar organic additives and alkali metal ions. Chem. Commun., 579–580.

[11] Ryoo, R., Joo, S.H., and Kim, J.M. (1999) Energetically Favored Formation of MCM-48 from Cationic–Neutral Surfactant Mixtures. J. Phys. Chem. B, 103, 7435-7440.

[12] Sayari, A. (2000) Novel Synthesis of High-Quality MCM-48 Silica.J. Am. Chem. Soc., 122, 6504-6505.

[13] Xia, Y.D. and Mokaya, R. (2003) Facile and high yield synthesis of mesostructured MCM-48 silica crystals. J. Mater. Chem., 13, 657-659.

[14] Kumar D., Schumarcher, K., Hohenesche, C., Grün, M., and Unger, K.K. (2001) MCM-41, MCM-48 and related mesoporous adsorbents: their synthesis and characterization. Colloids. Surf. A 187–188, 109–116.

[15] Kim, T.W., Chun, P.W., and Lin, V.S.Y. (2010) Facile Synthesis of Monodisperse Spherical MCM-48 Mesoporous Silica Nanoparticles with Controlled Particle Size.Chem. Mater., 22, 5093–5104.

[16] Wang,L., Shao, Y., Zhang, J., and Anpo, M. (2006) Synthesis of MCM-48 mesoporous molecular sieve with thermal and hydrothermal stability with the aid of promoter anions. Micropor. Mesopor. Mater., 95, 17–25.

[17] Wang, L., Zhang, J., and Chen, F. (2009) Synthesis of hydrothermally stable MCM-48 mesoporous molecular sieve at low cost of CTAB surfactant.Micropor. Mesopor. Mater., 122, 229–233.

[18] Phiriyawirut, P., Magaraphan, R., Jamieson, A.M., and Wongkasemjit, S. (2003) MFI zeolite synthesis directly from silatrane via sol–gel process and microwave technique.Mater. Sci. Eng. A, 361, 147–154.

[19] Charoenpinijkarn, W., Suwankruhasn, M., Kesapabutr, B., Wongkasemjit, S., and Jamieson, A.M. (2001) Sol–gel processing of silatranes. Eur. Polym. J., 37, 1441–1448.

[20] Sathupanya, M., Gulari, E., and Wongkasemjit, S. (2002) ANA and GIS Zeolite Synthesis Directly from Alumatrane and Silatrane by Sol–Gel Process and Microwave Techniques. J. Eur. Ceram. Soc., 22, 1293–1303.

[21] Sathupanya, M., Gulari, E., Wongkasemjit, S. (2003) Na-A (LTA) Zeolite Synthesis Directly from Alumatrane and Silatrane by Sol–Gel Microwave Techniques.J. Eur. Ceram. Soc., 23, 2305–2314.

[22] Phonthammachai, N., Chairassameewong, T., Gulari, E., Jameison, A.M., and Wongkasemjit, S. (2003) Oxide one pot synthesis of a novel titanium glycolate and its pyrolysis. J. Met. Mater. Min., 12, 23.

[23] Phiriyawirut, P., Jamieson, A.M., and Wongkasemjit, S. (2005) VS-1 zeolite synthesized directly from silatrane. Micropor. Mesopor. Mater., 77, 203–213.

[24] Thanabodeekij, N., Tanglumlert, W., Gulari, E., and Wongkasemjit, S. (2005) Synthesis of Ti-MCM-41 directly from silatrane and titanium glycolate and its catalytic activity. Appl. Organomet. Chem., 19, 1047–1054.

[25] Thanabodeekij, N., Sadthayanon, S., Gulari, E., and Wongkasemjit, S. (2006) Extremely high surface area of ordered mesoporous MCM-41 by atrane route. Mater. Chem. Phys., 98, 131–137.

[26] Mintova, S. and Čejka, J. (2007) Chapter 9 Micro/mesoporous composites. Stud. Surf. Sci. Catal., 168, 301–326.

[27] Cejka, J. and Mintova, S. (2007) Perspectives of Micro/Mesoporous Composites in Catalysis. Catal. Rev., 49, 457–509.

[28] Perez-Ramírez, J., Christensen, C.H., Egeblad, K., Christensen, C.H., and Groen, J.C. (2008) Hierarchical zeolites: enhanced utilisation of microporous crystals in catalysis by advances in materials design. Chem. Soc. Rev., 37, 2530–2542.

[29] Phiriyawirut, P., Magaraphan, R., Jamieson, A.M., and Wongkasemjit, S. (2003) Morphology study of MFI zeolite synthesized directly from silatrane and alumatrane via the sol–gel process and microwave heating. Micropor. Mesopor. Mater., 64(1–3), 83–93.

[30] Kruk, M., Jaroniec, M., Peña, M.L., and Rey, F. (2002) Determination of phase composition of MCM-48/lamellar phase mixtures using nitrogen adsorption and thermogravimetry. Chem. Mater., 14, 4434–4442.

[31] Roth, W.J. (2009) Facile synthesis of the cubic mesoporous material MCM-48. Detailed study of accompanying phase transformations. Adsorption, 15, 221–226.

[32] Chang, Z., Zhu, L., and Kevan, L. (1999) Electron Spin Resonance of Ni(I) in Ni−Containing MCM-41 Molecular Sieves. J. Phys. Chem. B, 103, 9442-9449.

[33] Xu, J., Luan, Z., He, H., Zhou, W., and Kwvan, L. (1998) A Reliable Synthesis of Cubic Mesoporous MCM-48 Molecular Sieve. Chem. Mater., 10, 3690–3698.

[34] Taralkar, U.S., Jha, R.K., and Joshi, P.N. (2007) Structural evolutions of hydrothermally prepared mesostructured MCM-48 silica using differently manufactured amorphous silica powders. J. Non. Cryst. Solids., 353, 194–199.

[35] Taralkar, U.S., Kasture, M.W., and Joshi, P.N. (2008) Influence of synthesis conditions on structural properties of MCM-48.J. Phys. Chem. Solids., 69, 2075–2081.

[36] Wei, F.Y., Liu, Z.W., Lu, J., and Liu, Z.T. (2010) Synthesis of mesoporous MCM-48 using fumed silica and mixed surfactants. Micropor. Mesopor. Mater., 131, 224–229.

[37] Sing, K.S.W., Everett, D.H., Houl, R.A.W., Moscou, L., Pierotti, R.A., Rouquerol, J., and Siemieniewska, T. (1985) Reporting physisorption data for gas/solid systems- with special reference to the determination of surface area and porosity. Pure. Appl. Chem., 57, 603.

[38] Petitto, C., Galarneau, A., Driole, M.F., Chiche, B., Alonso, B., Renzo, F.D., and Fajula, F. (2005) Synthesis of Discrete Micrometer-Sized Spherical Particles of MCM-48.Chem. Mater., 17, 2120–2130.

[39] Tanglumlert, W., Imae, T., White, T.J., and Wongkasemjit, S. (2007) Structural Aspects of SBA-1 Cubic Mesoporous Silica Synthesized via a Sol–Gel Process Using a Silatrane Precursor. J. Am. Ceram. Soc., 90(12), 3992–3997.

[40] Lysenko, N.D., Shvets, A.V., and Il'in, V.G. (2008) Field of concentrations and conditions of template structure formation of a silica mesoporous molecular sieves of MCM-48 type. Theor. Exp. Chem., 44, 195–199.

[41] Yu, J., Shi, J.L., Wang, L.Z., Gao, J.H., and Yan, D.S. (2000) Synthesis of MCM-48 under low surfactant/silicon molar ratio conditions. J. Mater. Sci. Lett., 19, 1461–1464.

[42] Park, S. H., Song, B. Y. and Lee, T. G. (2008) Effects of surfactant/silica and silica/cerium ratios on the characteristics of mesoporous Ce-MCM-41. J. Ind. Eng. Chem., 14(2), 261-264.

[43] Behrens, P., Glaue, A., Haggenmüller, C., and Schechner, G. (1997) Structure-directed materials syntheses: Synthesis field diagrams for the preparation of mesostructuredsilicas. Solid state Ionics, 101–103, 255–260.

[44] Collart, O., Van Der Voort, P., Vansant, E.F., Desplantier, D., Galarneau, A., Di Renzo, F., and Fajula, F. (2001) A high-yield reproducible synthesis of MCM-48 starting from fumed silica. J. Phy. Chem. B, 105, 12777–112771.

[45] Díaz, I., Pérez-Pariente, J., and Terasaki, O. (2004) Structural study by transmission and scanning electron microscopy of the time-dependent structural change in M41S mesoporous silica (MCM-41 to MCM-48, and MCM-50). J. Mater. Chem., 14, 48–53.

[46] Alfredsson, V., Anderson, M.W., Ohsuna, T., Terasaki, O., Jacob, M., and Bojrup, M. (1997) Cubosome Description of the Inorganic Mesoporous Structure MCM-48.Chem. Mater., 9, 2066–2070.

[47] Schumacher, K., Ravikovitch, P.I., Chensne, A.D., Neimark, A.V., and Unger, K.K. (2000) Characterization of MCM-48 Materials. Langmuir, 16, 4648–4654.

[48] Zhao, W., Li, Q., Wang, L., Chu, J., Qu, J., Li, S., and Qi, T. (2010) Synthesis of High Quality MCM-48 with Binary Cationic−Nonionic Surfactants. Langmuir, 26(10), 6982–6988.

Table 3.1 The characteristics of the calcined samples prepared at 140 °C with different crystallization time (16h, 20, and 24 h) using molar gel composition of SiO_2:0.65CTAB:0.5NaOH:62H_2O

Crystallization time (h)	S_{BET} (m^2/g)	Pore size (nm)	Pore volume (cm^3/g)	Unit cell a_0 (nm)	Wall thickness (nm)
16	1365	2.3	0.78	8.62	1.65
20	1148	2.6	0.75	8.69	1.51
24	921	2.9	0.68	8.59	1.31

Table 3.2 The characteristics of the calcined samples synthesized with the different CTAB/SiO_2 ratios

Amount of CTAB x mol	S_{BET} (m^2/g)	Pore size (nm)	Pore volume (cm^3/g)	*d* spacing (nm)
x = 0.65	1365	2.28	0.78	3.52
x = 0.55	1168	2.85	0.83	3.55
x = 0.40	1291	2.76	0.89	3.67
x = 0.35	1258	2.99	0.94	3.70
x = 0.30	1288	2.86	0.92	3.71
x = 0.25	720	2.41	0.44	3.58
x = 0.20	817	2.39	0.5	3.59
x = 0.15	-	-	-	3.52

Table 3.3 The effect of the alkalinity on the physical characteristics of a calcined MCM-48

	Alkalinity		
	0.45	**0.50**	**0.55**
Pore diameter	29.8 Å	28.6 Å	25.6 Å
Pore volume	0.96 cm^3/g	0.92 cm^3/g	0.87 cm^3/g
Wall thickness	13.3 Å	15.1 Å	14.3 Å

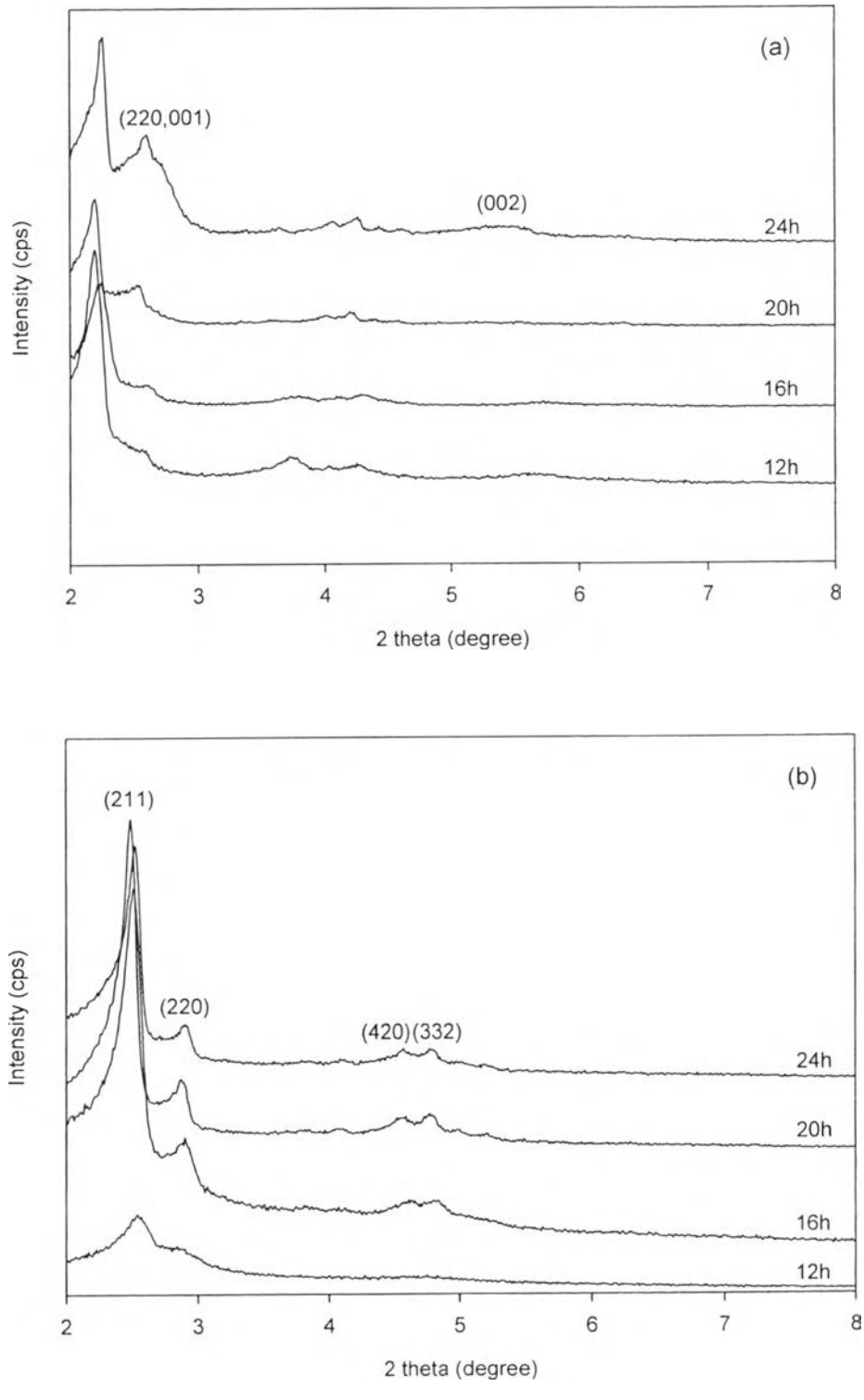

Figure 3.1 XRD-patterns of (a) the as-synthesized samples and (b) the calcined samples prepared at 140 °C for 12,16, 20 and 24 h.

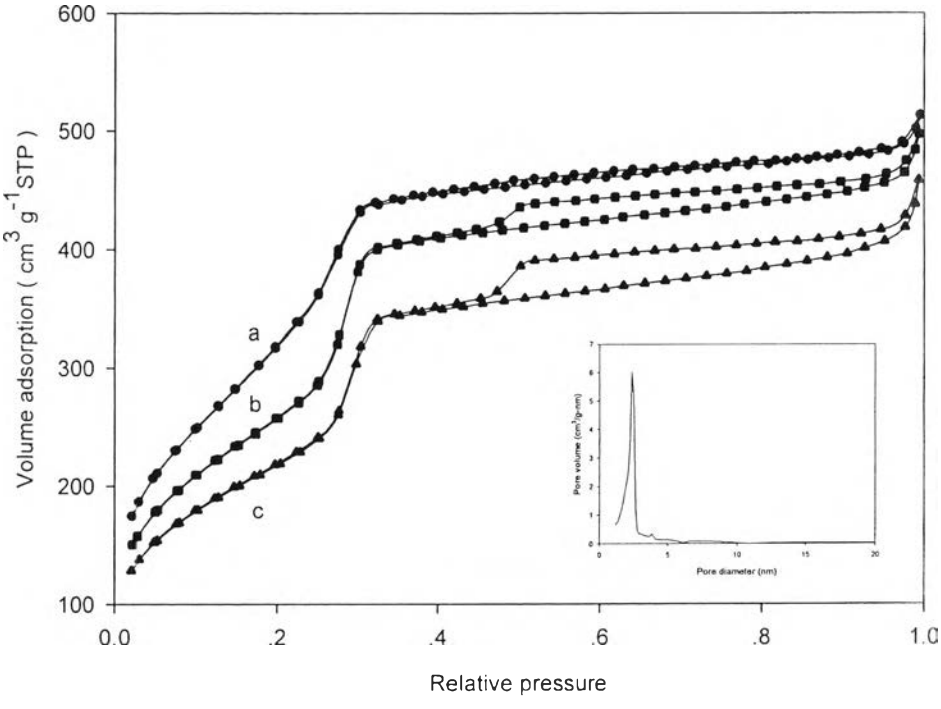

Figure 3.2 N_2-adsorption and desorption isotherms of the calcined samples prepared at 140 °C for 16, (b) 20, and (c) 24 h. The inset shows the BJH pore size distribution of calcined sample (a) calculated from the desorption branch of isotherm.

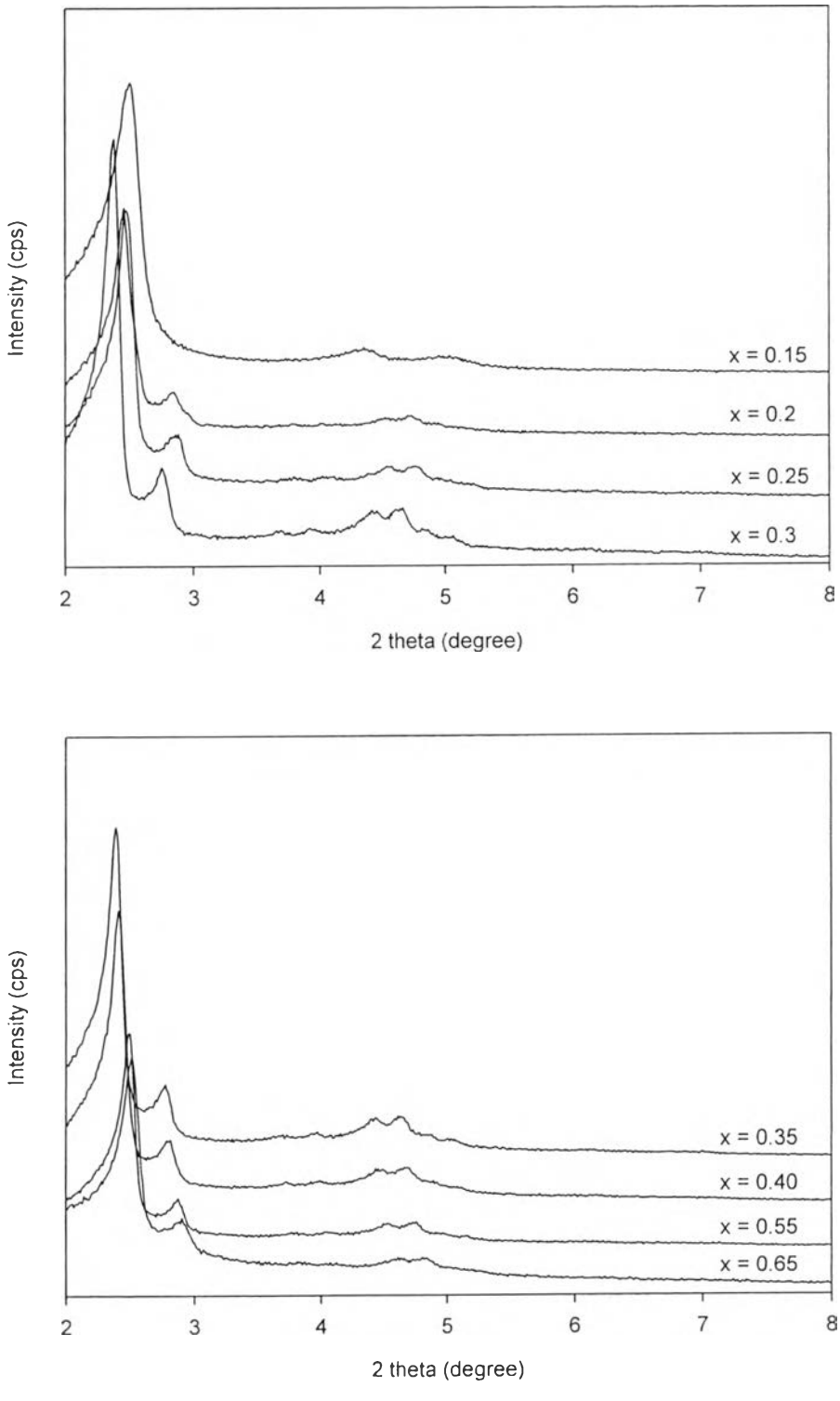

Figure 3.3 XRD-patterns of the calcined samples prepared at 140 °C for 16 h with molar gel composition of SiO_2:xCTAB:0.5NaOH:62H_2O, where $0.15 \leq x \leq 0.65$.

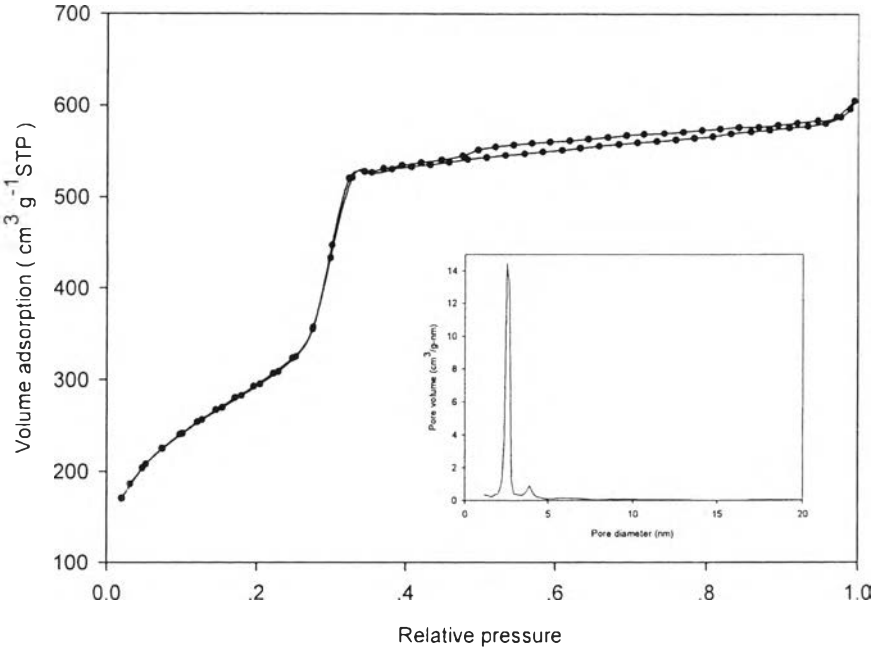

Figure 3.4 N_2-adsorption and desorption isotherms and pore size distribution (inset) of the calcined samples prepared at 140 °C for 16 h with molar gel composition of SiO_2:0.3CTAB:0.5NaOH:62H_2O.

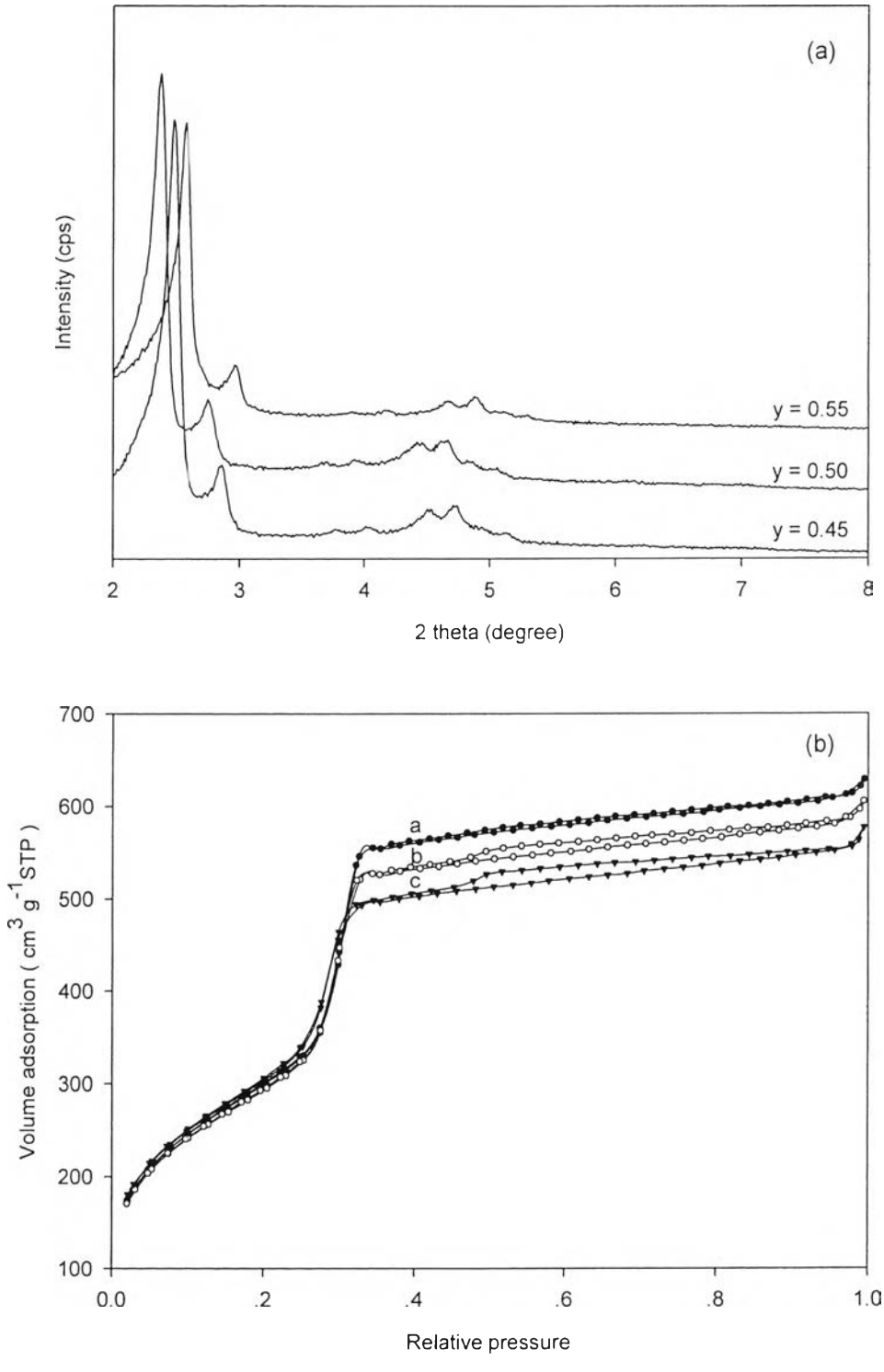

Figure 3.5 (a) XRD-patterns and (b) N_2-adsorption and desorption isotherms of the calcined samples prepared at 140 °C for 16 h with molar gel composition of SiO_2:0.3CTAB:yNaOH:62H_2O, where y is *a* 0.45, *b* 0.5, and *c* 0.55.

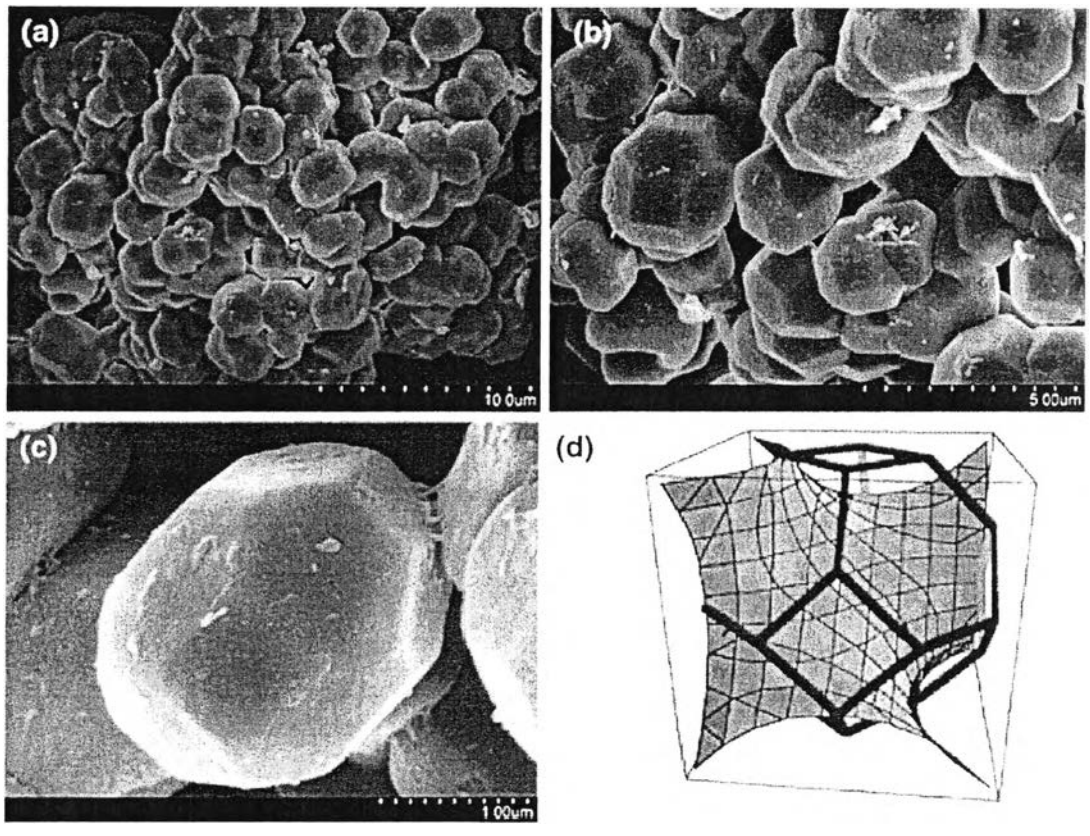

Figure 3.6 (a-c) FE-SEM images of MCM-48 synthesized with a molar gel composition of SiO_2:0.3CTAB:0.5NaOH:62H_2O at 140 °C for 16 h. (d) Schematic representation of the gyroid surface according to space group *Ia3d* divides a regular truncated octahedron in two, cutting six of the eight hexagonal faces [44].

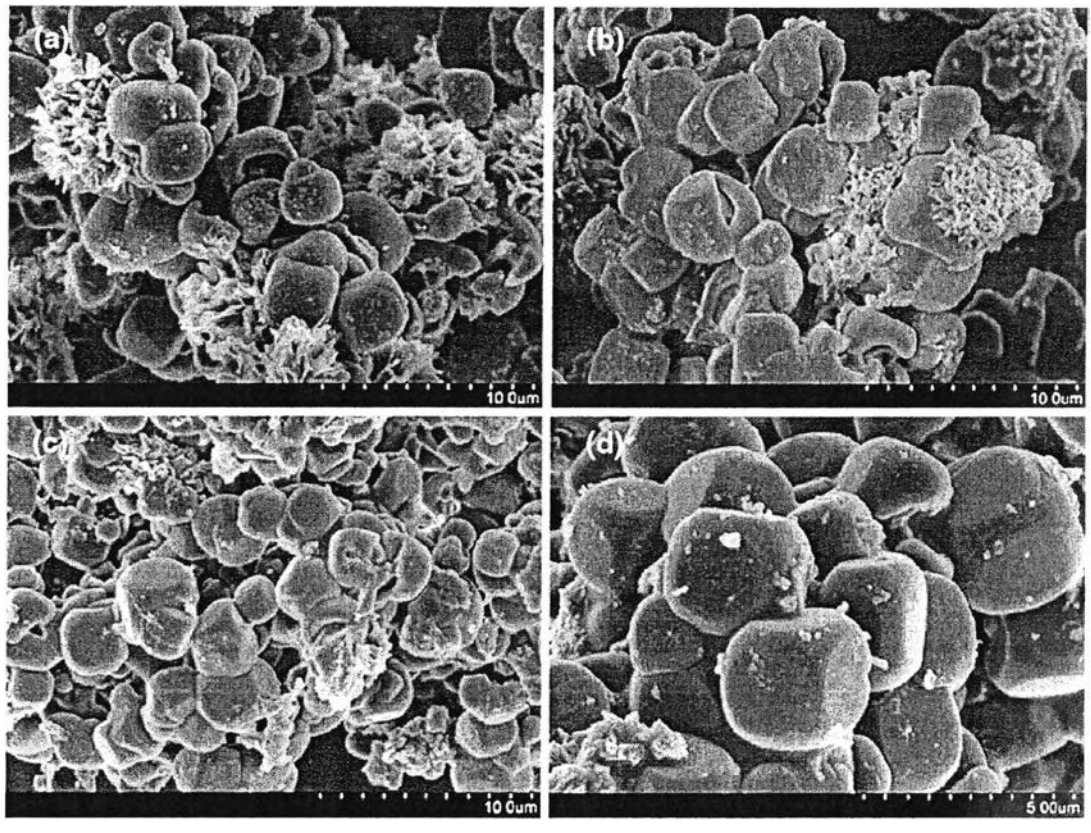

Figure 3.7 FE-SEM images of MCM-48 synthesized with a molar gel composition of SiO_2:0.65CTAB:0.5NaOH:62H_2O at 140 °C for (a) 24, (b) 20, (c) 16 (x5000), and (d) 16 h (x10000).

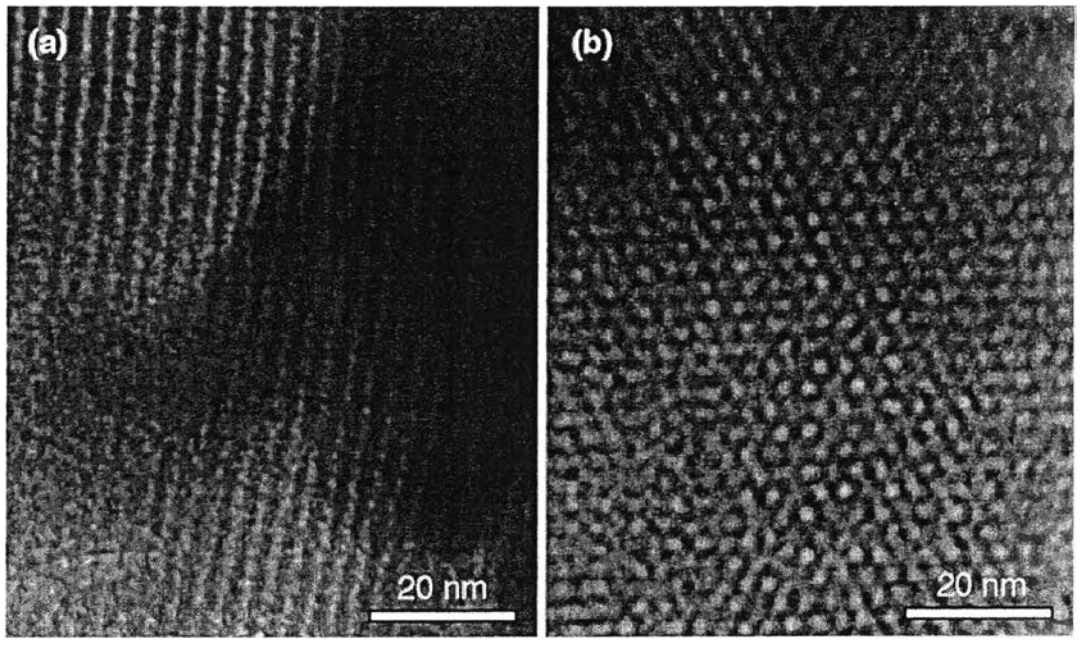

Figure 3.8 TEM images of MCM-48 synthesized with a molar gel composition of SiO_2:0.3CTAB:0.5NaOH: $62H_2O$ at 140 °C for 16 h with incident direction along (a) [110] and (b) [111].